Heteroatom Framework Distribution and Layer Charge of Sodium Taeniolite

Ana C. Perdigón[1], Carmen Pesquera[1], Agustín Cota[2], Francisco J. Osuna[3], Esperanza Pavón[3], María D. Alba[3*]

[1] Departamento de Química e Ingeniería de Procesos y Recursos. Universidad Cantabria. Avda. Los Castros s/n. 39005 Santander (Spain)

[2] Laboratorio de Rayos-X. Centro de Investigación, Ciencia y Tecnología de la Universidad de Sevilla (CITIUS). Avda. Reina Mercedes, 4. 41012 Sevilla (Spain)

[3] Instituto Ciencia de los Materiales de Sevilla (CSIC-US). Avda. Reina Mercedes, 49. 41092 Sevilla (Spain)

ABSTRACT

The most advanced applications of clays depend crucially on their hydration state and swelling is probably the most important feature of expandable 2:1 layered silicate. Sodium Taeniolite, Na-TAE, a swelling trioctahedral fluormica, has been synthesized and studied using thermogravimetric analysis, X-ray diffraction, scanning electron microscopy and infrared and solid state NMR spectroscopies. The results indicated the formation of a swelling 2:1 phyllosilicate with actual layer charge lower than the nominal one. Herein, a new heteroatom distribution and more accurate composition could be deduced.

1. Introduction

Swelling silicates of the 2:1 phyllosilicate family with low negative charge are 2D host materials with multiple and diverse physicochemical applications going from the well-known catalysis (Alves et al., 2014; Breu et al., 1999; Centi and Perathoner, 2008; Cheng, 1999; Thomas, 1988; Vaccari, 1999) and adsorption/separation (Barrer, 1989; Mercier and Pinnavaia, 1998; Okada and Ogawa, 2017; Tomohiko et al., 2014) to the latest nanotechnology (Schollhorn, 1996; Schoonheydt and Umemura, 2017), sensor technology (Mallouk and Gavin, 1998) and optoelectronics.(Kunz et al., 2013; Lezhnina et al., 2007).

Chemical structure is the ultimate responsible of those interesting applications. The structure, an octahedral sheet sandwiched between two tetrahedral sheets, is extremely flexible to isomorphic substitutions. Additionally, the interlayer cation can be substituted by cation exchange reactions and large inorganic or organic molecules can be introduced in the interlayer space giving those materials a wide adaptability.

Chemical reactivity and stability in the interlayer space as a reaction media strongly depends not only of the layer charge but also from its origin (Alba et al., 2001a, b; Alba et al., 2010; Alba et al., 2009; Chain et al., 2013). On the one hand, cation substitutions on tetrahedral sheet favor reconstructive reactions under subcritical conditions (Alba et al., 2001a). On the other hand, cation substitutions on octahedral sheet provides an excess of negative charge that is delocalized in the framework (Sposito and Prost, 1982), and, thus, a more homogeneous distribution of cations in the interlayer space. Moreover, the hydration properties of 2:1 phyllosilicates are also governed by those structural features because their swelling behaviour depends on the repulsive forces relating to the interactions between the 2:1 layers and the attractive

forces between the interlayer cation and the negative charged siloxane surface (Pavon et al., 2014).

True and brittle natural micas constitute a major group of those 2D host materials but layer charge is high and strong Coulomb interactions with interlayer cations usually inhibit their swelling and hence, a very low cation-exchange capacity (CEC) results and limits applicability. However, as will be shown in the following, swelling high-charge micas can be easily synthesized and their CEC tuned via the degree of isomorphous substitution, broadening their wide-ranging uses.

Depending on the origin of the layer charge, two family of swelling mica can be found. First, synthetic fluorine micas have been recently synthetized (Alba et al., 2006) that are able to swell despite their high layer charge originated in the tetrahedral sheet by Si/Al replacements (Alba et al., 2006; Naranjo et al., 2015; Pavon et al., 2013). Consequently, those materials, referred as Na-*n*-Mica or Na-Mica-*n* (being *n* the layer charge and related to the ratio Si/Al) have potential used as decontaminants and storage media (Alba et al., 2006; Garcia-Jimenez et al., 2016; Gregorkiewitz and Rausell-Colom, 1987; Park et al., 2002; Paulus et al., 1992).

Second, synthetic sodium Taeniolite, an analogous of the swelling fluoromica Na-Mica-2, where substitutions in the octahedral sheet (Mg/Li) are the ultimate responsible of layer charge (Kitajima et al., 1985; Kitajima and Takusagawa, 1990; Kitajima et al., 1991). Sodium Taeniolite ($NaSi_4Mg_2LiO_{10}F_2 \cdot xH_2O$) exhibits reversible swelling (Toraya et al., 1977) and Kitajima *et al.* (Kitajima et al., 1973) explained its swelling characteristics by the high hydration energy of the interlayer sodium ions. Taeniolite derivatives are interesting microporous host materials that can be used as sensors for redox-active ambient gas (Baumgartner et al., 2008; Mariychuk et al., 2007).

The capability of the 2:1 structure to vary the framework chemical composition and heteroatom distribution is crucial to design new materials with desired properties; however, it leaves one worrying about the homogeneity of the synthesized material. In many cases, the charge densities vary not only from one silicate layer to other in a crystallite (Lagaly, 1994) but also from domain to domain within a single silicate layer (Muller et al., 1997) and this heterogeneous distribution of negative charge influences the distribution cations in the interlayer space (Breu et al., 1999).

The charge density of the silicate layers is of utmost importance for the properties of the material. Na-Mica-n have been extensively analysed (Alba et al., 2006) but, to our knowledge, the only available information of Na-Taeniolite is related to their crystalline order and swelling capacity (Kitajima et al., 1985; Kitajima et al., 1973; Miyake et al., 1993; Moore et al., 1997; Toraya et al., 1977). Thus, the goal of this research was to shed some light on the uniformity of their composition, charge density, and interlayer composition by the combination of characterization techniques that provide structural information at long and short range.

2. Experimental section

2.1.Synthesis method.

The reagents of SiO_2 (Sigma, 99.8% CAS Nº 112945-52-5), LiF (Aldrich, 99.99%, CAS Nº 1309-48-4), MgO (Aldrich, 99.9%, CAS Nº 1309-48-4) and NaF (Aldrich, 99.0%, CAS Nº 7681-49-4) were dried at 100 ºC for 24 h and carefully weighed out according to the formulae $[Na_2][Si_8][Mg_{24}Li_2]O_{20}F_4$.

All reagents were mixed and vigorously ground before heating at 1100 °C in a Pt crucible for 2 h. After cooling up to 950 ºC, the solid was quenched to room

temperature (RT) and equilibrated at RT ambient humidity. The as-synthesized sample was named as Na-TAE.

2.2.Characterization.

TG/DTA experiment was carried out using a TA (model STD-Q600) instrument, in Characterization Service (CITIUS, University of Seville, Spain), with alumina as reference. The sample was placed into a Pt crucible and maintained at air throughout the heating period. The temperature was increased at a constant rate of 10° C/min.

Powder X-ray diffraction (XRD) was performed at the X-ray laboratory (CITIUS, University of Seville, Spain) on a Bruker D8 Advance Bragg-Brentano instrument equipped with a Cu K_α radiation source operating at 40 kV and 40 mA. The diffractogram was obtained in the 2θ range of 3–70° with a step size of 0.015° and a step time of 0.1 s.

FTIR spectrum was recorded in the range 4000–300 cm^{-1} by the Spectroscopy Service of the ICMS (CSIC-US, Seville, Spain), as KBr pellets, using a Nicolet spectrometer (model 510P) with a nominal resolution of 4 cm^{-1}.

The morphology of the sample was analyzed by Scanning Electron Microscopy, SEM, (JEOL, Model JSM 5400) at 20kV in the Microscopy Service of ICMS (CSIC-US). An EDX system (Oxford Link ISIS) was fitted to the SEM equipment to perform chemical analyses of the sample using a Si/Li detector with Be window.

Single-pulse (SP) MAS NMR spectra were recorded in the Nuclear Magnetic Resonance Unit at the University of Cordoba (Spain) on a Bruker AVANCE WB400 spectrometer equipped with a multinuclear probe. Powdered sample was packed in 3.2 mm zirconia rotors and spun at 10 kHz. ^{29}Si MAS NMR spectrum was acquired at a frequency of 79.49 MHz, using a pulse width of 2.7 μs (π/2 pulse length = 7.1 μs) and

delay times of 3 s. ^{6}Li MAS NMR spectrum was recorded at 58.86 MHz with a pulse width of 0.9 µs (π/2 pulse length = 1.8 µs) and a delay time of 30 s, in this case the rotor was spun at 14 kHz to improve the spectral resolution. ^{23}Na MAS NMR spectrum was recorded at 105.84 MHz with a pulse width of 0.75 µs (π/2 pulse length = 4.5 µs) and a delay time of 0.1 s. The ^{19}F MAS spectrum was obtained using typical π/2 pulse widths of 2.9 µs and a pulse space of 2 s. The chemical shift values were reported in ppm from tetramethylsilane for ^{29}Si, from NaF for ^{19}F and from a 0.1 M LiCl and NaCl solution for ^{6}Li and ^{23}Na, respectively. Spectra were simulated using the DMFIT software (Massiot et al., 2002). A Gaussian-Lorentzian model was used for all peaks, and linewidth, position and amplitude were the fitted parameters.

3. Results and discussion

The XRD pattern (Fig. 1) is similar to the previously reported for the one-layer hydrated 2:1 structure of Na-Taeniolite (Miyake et al., 1993; Suzuki et al., 2008; Yamaguchi et al., 2012) and showed a sharp *001* diffraction peak at 7.2º 2θ (d_{001}=12.2 Å) and high order *00l* reflections corresponding to the single-layer hydrate state of the interlayer cations (Kitajima et al., 1985). Kalo et al. (Kalo et al., 2010) also observed that $Na_{0.6}$-fluorohectorite spontaneously absorbs air moisture to form a monolayer hydrate (ca. 2 H_2O per unit cell) at ambient conditions. Additionally, some reflections due to protoamphibole (PDF 00-013-0409), an orthorhombic fluoroamphibole,(Gibbs et al., 1960) are detected in the XRD patterns, as previously reported for Na-fluorohectorite (Kitajima et al., 1985). Also, Yamaguchi et al. (Yamaguchi et al., 2012) observed some impurities in Taeniolite obtained from Na-rich raw batches (≥ 3 mol NaCl) that they could not identify and nor remove after rigorous washing.

Fig. S1 showed the c-axis projection of the K-Taeniolite structure (Toraya et al., 1977) and the a-axis projection of protoamphibole structure (Gibbs, 1969), the similarity of building blocks of both, protoamphibole being slightly denser, may favour that protoamphibole acts as a natural competitor for the 2:1 layer structure (Breu et al., 2001).

The hydration state of the Na-TAE was tested by thermogravimetric analysis (Fig. S2). In the region between 25 ºC and 150 ºC, where water molecules are desorbed, a unique weight lost was observed with the maximum in the DTG curve at 66 ºC, associated to a 4.92 % of weight loss. If the ideal formula, $Na_2Si_8Mg_4Li_2O_{20}F_4 \cdot xH_2O$, is taken into account this weight loss corresponds to 2.23 H_2O per unit cell. This value is low as previously reported for Na-Taeniolite (Miyake et al., 1993), $Na_{0.6}$-fluorohectorite (Kalo et al., 2010) and for Na-Mica-2, a fluoromica with layer charge originated in the tetrahedral sheet instead of in the octahedral one (Gregorkiewitz and Rausell-Colom, 1987; Kalo et al., 2013; Pavon et al., 2013). The low water weight loss is justified by the coordination of the interlayer cation to the basal oxygen of the tetrahedral sheet and, maybe, fluorine (Rayner-Canham and Overton, 2006).

The morphology of the sample was analysed by scanning electron microscopy (Fig. 2) which shows that most particles have a lamellar structure compatible with the 2:1 phyllosilicate, Na-TAE, (image a). The EDX spectrum (spectrum a) shows lines compatible with chemical composition of Na-TAE but the semiquantitative analysis of the peaks intensities reveals that Mg/Si and Na/Si ratios are lower than that expected for Na-TAE-2 (Mg/Si=0.35 vs 0.50 and Na/Si=0.07 vs 0.25). Particles with a denser morphology (image b) was observed that can be attributed to the protoamphibole detected by XRD and its EDX spectrum shows lines compatible with it chemical composition (spectrum b).

Once confirmed the hydrated laminar structure of Na-TAE, the tetrahedral lattice vibrations were analysed by IRFT spectroscopy (Fig. 3) because they are affected by the magnitude of the layer charge and/or by the changes in octahedral and interlayer compositions (Kitajima et al., 1985; Kitajima and Takusagawa, 1990; Kitajima et al., 1991). The IRFT spectrum in this region showed absorption bands at ca. 980 and 1102 cm^{-1} assigned to e_1^1 and a_1^1, stretching Si-O_a, mode (Kitajima et al., 1985; Kitajima and Takusagawa, 1990) and a band at ca. 715 cm^{-1} due to a_1^2 mode (Yamaguchi et al., 2012). Consequently, judging from the IR spectra, the Na-TAE has similar chemical composition reported in the literature for Na-Taeniolite (Yamaguchi et al., 2012).

The local structure of the heteroatoms in the framework and in the interlayer space was studied by MAS NMR of the ^{29}Si, ^{19}F, ^{6}Li and ^{23}Na nuclei (Fig. 4); the spectra were deconvoluted and the fitting parameters (Table 1) were assigned to structural features.

The ^{29}Si MAS NMR spectrum shows a main signal at -91.37 ppm and two minor signals at -85.07 and -83.39 ppm. The main signal resonates in the region of $Q^3(0Al)$ (Sanz et al., 2006) as due to the 2:1 phyllosilicate (Na-TAE) and the minors contributions resonated in the region of Q^2 and is compatible with Si in protoamphibole (Welch et al., 1998), the impurity observed by XRD. The percentage of the area of the peaks (Table 1) indicate that only a 5% of the Si atoms corresponds to protoamphibole.

The ^{19}F spectrum is characterized by three signals at -177.39, -183.53 and -189.44 ppm, corresponding to F(Mg-Mg-Mg), F(Mg-Mg-Li) and F(Mg-Li-Li), respectively (Huve et al., 1992; Kaviratna and Pinnavaia, 1994; Keenan et al., 2013; Labouriau et al., 1995). The spectral deconvolution is performed to obtain quantitative information of the relative $[Mg^{2+}]_3$ to $[Mg^{2+}][Li^{+}]_2$ environmental populations (see Table 1). From signal intensities, a Mg^{2+}/Li^{+} ratio equals to 3.20 is calculated and it is

representative of a layer charge equals to ca. -1.43. Therefore, the formulae would be approximately rewritten as $M_{1.43}[Si_8][Mg_{4.57}Li_{1.43}]O_{20}F_4$, where M=Na and/or Li.

The assumption of a layer charge lower than the nominal layer charged can be corroborated by a deep analysis of the signals´ chemical shits from the ^{29}Si MAS NMR spectrum (Komarneni et al., 2005). As previously reported in the literature, ^{29}Si chemical shift in 2:1 phyllosilicates is quite sensible to layer charge, origin of the charge and the anion of octahedral coordination sphere (OH or F) (Alba et al., 2006; Keenan et al., 2013; Sanz et al., 2006). The correlation between chemical shift (δ) and the absolute value of the layer charge (x) in Fig. 5 uses data from literature (Alba et al., 2006; Gerstmans et al., 2008; Keenan et al., 2013; Sanz et al., 2006) and analyses structural features. The anion nature of the octahedral sheet, OH or F, (filled star vs filled circle); the nature of the octahedral cation (pink vs purple stars and blue vs cyan circles) and the nature of the interlayer cation (blue circle vs. blue triangle and purple star vs. purple triangle) are analyzed. The relation between the chemical shift and absolute value of layer charge depends mainly on the first two factors, therefore, four grouped data can be set up and four linear correlations calculated:

Line I: $\delta=-98.25+2.88\cdot x$, $R^2=0.983$ (OH and Mg in octahedral sheet)

Line II: $\delta=-98.29+2.66\cdot x$, $R^2=0.911$ (OH and Mg-Al in octahedral sheet)

Line III: $\delta=-97.52+3.61\cdot x$, $R^2=0.942$ (F and Mg-Li in octahedral sheet)

The set of chemical shift fitting with Line III corresponds to 2:1 phyllosilicate with the most similar composition to Na-TAE. Consequently, this equation has been employed for a semiquantitative estimation of the layer charge of Na-TAE, returning a value $\leq$ -1.70, lower than the nominal value of -2. In the literature (Kitajima and Daimon, 1972; Kondo et al., 1980; Yamaguchi et al., 2012), a layer charge equal to -2 was assumed on the base of the nominal stoichiometry of the reaction mixture. In this

sense, Kitajima et al. (Kitajima et al., 1991) observed that the stretching Si-O_a in FTIR spectra shifted to lower frequency as layer charge increased, however, Na-Taeniolite reported in literature showed a slightly higher frequency (1110 cm^{-1}) (Yamaguchi et al., 2012) than Na-TAE reported here (1102 cm^{-1}), then those Na-Taeniolites could also exhibit a layer charger lower than -2.

Once known the actual framework heteroatom distribution, the analysis of the interlayer space has been performed thorough ^{23}Na and ^{6}Li MAS NMR. ^{23}Na MAS NMR spectroscopy is sensitive to the local environment and will not only be influenced by the hydration, but also by different planar defects in the stacking of the 2:1 layers (Moller et al., 2010). The ^{23}Na spectrum is characterized by a broad band that has been deconvoluted in four peaks (Table 1) and they correspond to one-layer hydrate (78.4 %) and poor hydrated exchangeable sodium (21.6%) (Naranjo et al., 2015). It should be noted that ^{23}Na is a quadrupolar nuclei with a half-integer spin and, therefore, affected by second order quadrupolar interaction. Nevertheless, it was almost eliminated by the rotor spun and the magnetic field and very small spinning side band are observed.

Finally, ^{6}Li MAS NMR spectrum is the overlapping of two resonances at 0.23 and -0.72 ppm, which can be due to hydrated interlayer lithium cation and lithium in the octahedral sheet of trioctahedral 2:1 phyllosilicates. Bond et al. (Bond et al., 1991) observed a unique signal in Na-Laponite at -0.73 ppm due to Li in octahedral sheet and tow signals when Na was exchanged by Li, being the new resonance more deshielded. It is remarkable that no resonance associated to poor hydrated lithium is observed and could be explained because of the tendency to form inner sphere complex for sodium (lower hydration state) is higher than that of lithium (Pavon et al., 2013). The proportion found between both location of lithium (Table 1), the ^{19}F MAS NMR and TG results

allow to estimate a Na-TAE composition such as: $Li_{0.91}Na_{0.52}[Si_8][Mg_{4.57}Li_{1.43}]O_{20}F_4 \cdot 2.18H_2O$.

4. Conclusions

For the first time, a short-range structural analysis was performed on sodium Taeniolite, which has allowed to shed a light on the distribution of the heteroatoms in the framework, to estimate the actual layer charge, which is lower than the nominal one and to propose a more accurate composition, $Li_{0.91}Na_{0.52}[Si_8][Mg_{4.57}Li_{1.43}]O_{20}F_4 \cdot 2.18H_2O$.

Additionally, the thermogravimetric results indicate a low water content, which is compatible with the presence of poor hydrated exchangeable interlayer sodium and sodium partially coordinated by basal oxygen of the tetrahedral sheet of the silicate.

Those results allow a deeper knowledge of the real Na-Taeniolite structure and hence, a better understanding of its promising properties.

ASSOCIATED CONTENT

Supporting Information

The Supporting Information is available free of charge on the ACS Publications webs. Figures include the K-Taeniolite and Protoamphibole structures and the DTG curve of Na-TAE.

AUTHOR INFORMATION

Corresponding Author

*E-mail: alba@icmse.csic.es

Notes

The authors declare no competing financial interest.

ACKNOWLEDGEMENT

The authors would like to thank the Junta de Andalucía (Spain) and FEDER (Proyecto de Excelencia de la Junta de Andalucía, project P12-FQM-567), to the Spanish State Program R+D +I oriented societal challenges and FEDER (Project MAT2015-63929-R) and ENRESA (contract nº 0079000237) for financial support. F.J. Osuna thanks his grant to the training researcher program associated to the excellence project of Junta de Andalucía (P12-FQM-567). Finally, Dr. Pavón thanks her grant to Andalucía Talent Hub Program, co-funded by the EU in 7FP, Marie Skłodowska-Curie actions (nº 291780) and the Junta de Andalucía.

284

285

286

287

288

289

Table 1.

Fit parameters of NMR spectra of Na-TAE.

	δ (ppm)	Fwhh (kHz)	%	assignation
^{29}Si	-83.39	0.20	3.5	Q^2 (protoamphibole)
	-85.07	0.12	1.3	Q^2 (protoamphibole)
	-91.37	0.18	95.2	Q^3(0Al)
^{19}F	-177.39	1.07	32.6	F(Mg-Mg-Mg)
	-183.53	1.42	63.4	F(Mg-Mg-Li)
	-189.44	1.06	4.0	F(Mg-Li-Li)
^{23}Na	-8.86	0.70	6.8	Fully hydrated
	-12.97	1.98	71.6	
	-31.35	1.95	15.2	Poor hydrated
	-49.53	1.61	6.4	
^{6}Li	0.23	0.06	39.0	Interlayer
	-0.72	0.03	61.0	Framework

FIGURE CAPTION

Fig. 1. XRD of Na-TAE. *=protoamphibole=00-013-0409

Fig. 2. SEM image and EDX spectra of Na-TAE: a) particles with layered morphology, and, b) particles with compacted morphology.

Fig. 3. IRFT spectrum of Na-TAE. The vibrational peaks have been labelled with the vibrations mode.

Fig. 4. ^{29}Si, ^{19}F, ^{6}Li and ^{23}Na MAS NMR spectra of Na-TAE.

Fig. 5. Chemical shift and absolute value of layer charge correlation of trioctahedral 2:1 phyllosilicates as a function of structural parameters, referred to $O_{20}F_4$ units. Symbols represents the experimental data from literature (Alba et al., 2006; Gerstmans et al., 2008; Keenan et al., 2013; Sanz et al., 2006), *oh* is the composition of the octahedral sheet, *i.s.* is the composition of the interlayer space and lines are the data fittings: blue line (line I), cyan line (line II) and purple line (line III).

306 **Fig. 1**

307

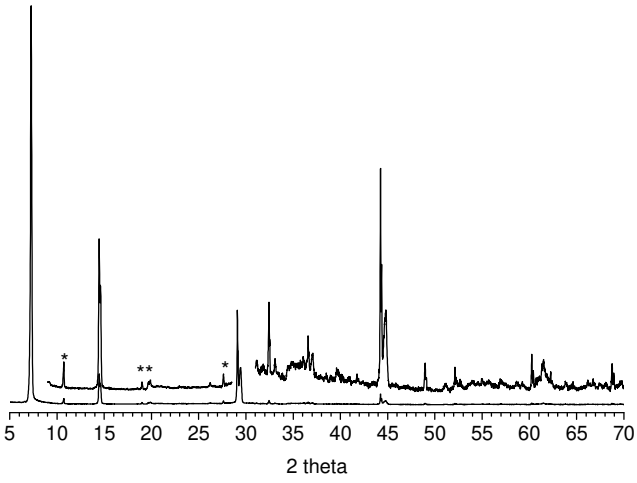

308

309

310 **Fig. 2**

311

312

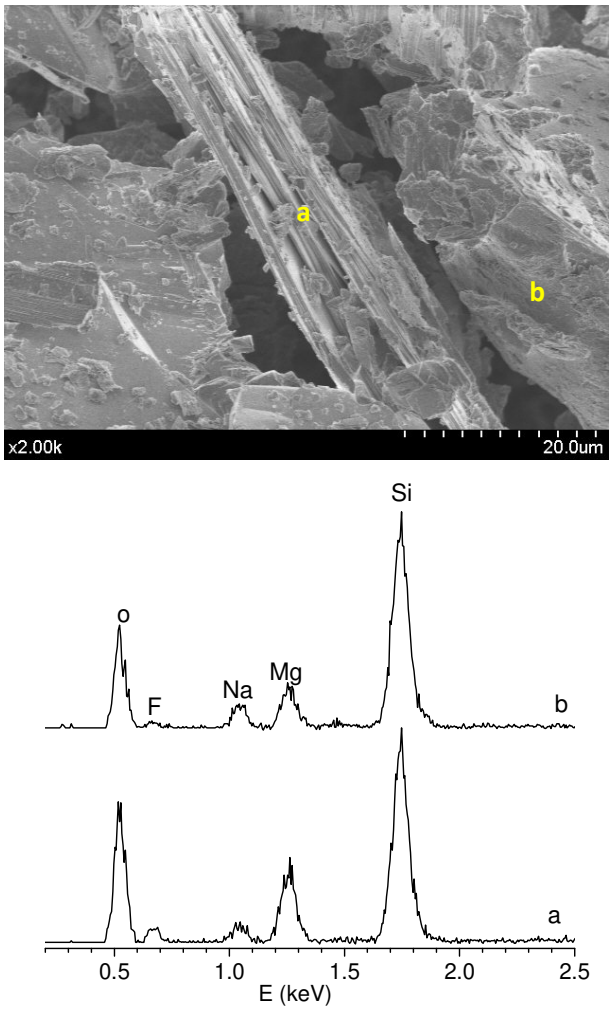

313 **Fig. 3**

314

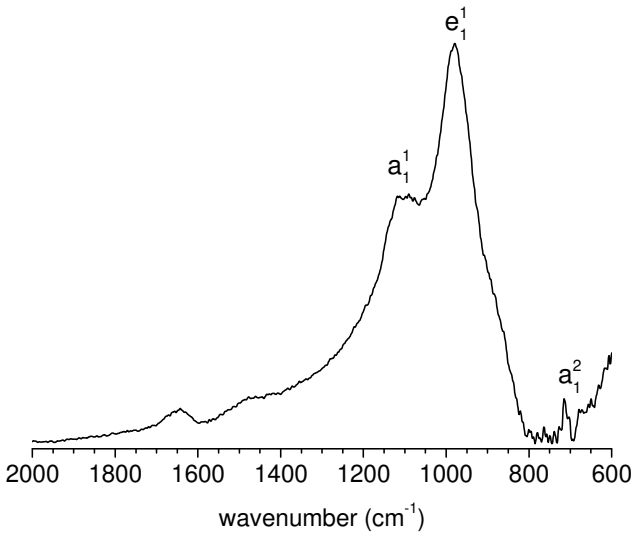

315

316 **Fig. 4**

317

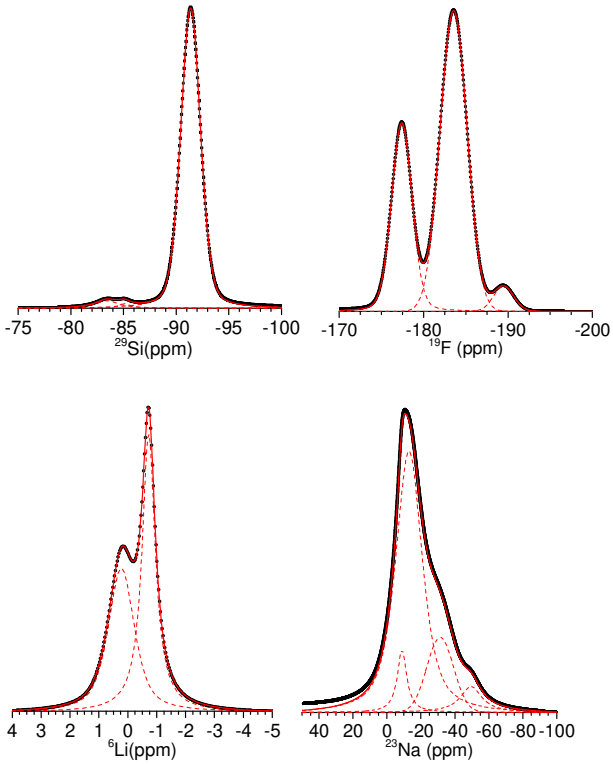

318

319

Fig. 5

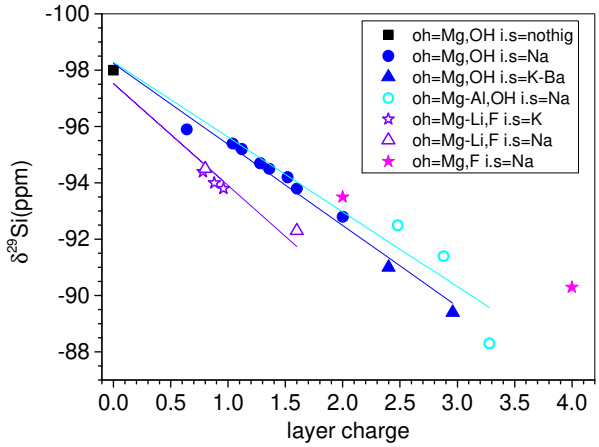
oh=Mg,OH i.s=nothig
oh=Mg,OH i.s=Na
oh=Mg,OH i.s=K-Ba
oh=Mg-Al,OH i.s=Na
oh=Mg-Li,F i.s=K
oh=Mg-Li,F i.s=Na
oh=Mg,F i.s=Na
δ29Si(ppm)
layer charge
-100
-98
-96
-94
-92
-90
-88
0.0
0.5
1.0
1.5
2.0
2.5
3.0
3.5
4.0

GRAPHICAL ABSTRACT

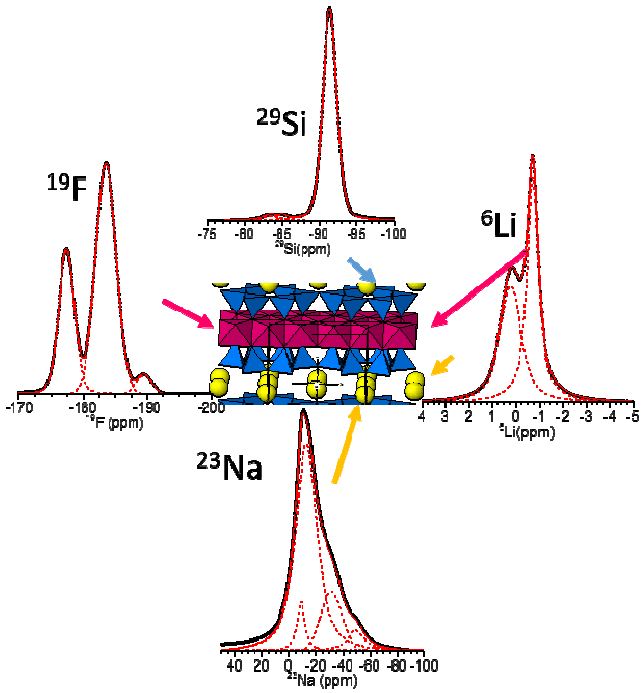

REFERENCE

Alba, M.D., Becerro, A.I., Castro, M.A., Perdigon, A.C., 2001a. Hydrothermal reactivity of Lu-saturated smectites: Part I. A long-range order study. Am. Miner. 86, 115-123.

Alba, M.D., Becerro, A.I., Castro, M.A., Perdigon, A.C., 2001b. Hydrothermal reactivity of Lu-saturated smectites: Part II. A short-range order study. Am. Miner. 86, 124-131.

Alba, M.D., Castro, M.A., Chain, P., Orta, M.M., Pazos, M.C., Pavon, E., 2010. HYDROTHERMAL STABILITY OF LAYERED SILICATES IN NEUTRAL AND ACIDIC MEDIA: EFFECT ON ENGINEERED-BARRIER SAFETY. Clay Clay Min. 58, 501-514.

Alba, M.D., Castro, M.A., Naranjo, M., Pavon, E., 2006. Hydrothermal reactivity of Na-n-micas (n=2, 3, 4). Chem. Mat. 18, 2867-2872.

Alba, M.D., Chain, P., Orta, M.M., 2009. Chemical reactivity of argillaceous material in engineered barrier Rare earth disilicate formation under subcritical conditions. Appl. Clay Sci. 43, 369-375.

Alves, H.J., da Rocha, A.M., Monteiro, M.R., Moretti, C., Cabrelon, M.D., Schwengber, C.A., Milinsk, M.C., 2014. Treatment of clay with KF: New solid catalyst for biodiesel production. Appl. Clay Sci. 91-92, 98-104.

Barrer, R.M., 1989. SHAPE-SELECTIVE SORBENTS BASED ON CLAY-MINERALS - A REVIEW. Clay Clay Min. 37, 385-395.

Baumgartner, A., Sattler, K., Thun, J., Breu, J., 2008. A route to microporous materials through oxidative pillaring of micas. Angewandte Chemie - International Edition 47, 1640-1644.

Bond, S.P., Gelder, A., Homer, J., McWhinnie, W.R., Perry, M.C., 1991. LI-6 MAGIC ANGLE SPINNING NUCLEAR-MAGNETIC-RESONANCE SPECTROSCOPY - A POWERFUL PROBE FOR THE STUDY OF LITHIUM-CONTAINING MATERIALS. J. Mater. Chem. 1, 327-330.

Breu, J., Raj, N., Catlow, C.R.A., 1999. Chiral recognition among trisdiimine-metal complexes, Part 4. Atomistic computer modeling of Ru(bpy)(3) (2+) and Ru(phen)(3) (2+) intercalated into low charged smectites. J. Chem. Soc.-Dalton Trans., 835-845.

Breu, J., Seidl, W., Stoll, A.J., Lange, K.G., Probst, T.U., 2001. Charge homogeneity in synthetic fluorohectorite. Chem. Mat. 13, 4213-4220.

Centi, G., Perathoner, S., 2008. Catalysis by layered materials: A review. Microporous Mesoporous Mat. 107, 3-15.

Chain, P., Cota, A., El Mrabet, S., Pavon, E., Pazos, M.C., Alba, M.D., 2013. Evaluation of rare earth on layered silicates under subcritical conditions: Effect of the framework and interlayer space composition. Chem. Geol. 347, 208-216.

Cheng, S., 1999. From layer compounds to catalytic materials. Catal. Today 49, 303-312.

Garcia-Jimenez, M.J., Cota, A., Osuna, F.J., Pavon, E., Alba, M.D., 2016. Influence of temperature and time on the Eu3+ reaction with synthetic Na-Mica-n (n=2 and 4). Chem. Eng. J. 284, 1174-1183.

Gerstmans, A., Urbanczyk, L., Jerome, R., Robert, J.L., Grandjean, J., 2008. XRD and NMR characterization of synthetic hectorites and the corresponding surfactant-exchanged clays. Clay Min. 43, 205-212.

Gibbs, G.V., 1969. Crystal structure of protoamphibole. Mineral. Soc. Amer. Spec. Pap. 2, 101-109.

375 Gibbs, G.V., Bloss, F.D., Shell, H.R., 1960. PROTO-AMPHIBOLE, A NEW
376 POLYTYPE. Am. Miner. 45, 974-989.
377 Gregorkiewitz, M., Rausell-Colom, J.A., 1987. CHARACTERIZATION AND
378 PROPERTIES OF A NEW SYNTHETIC SILICATE WITH HIGHLY CHARGED
379 MICA-TYPE LAYERS. Am. Miner. 72, 515-527.
380 Huve, L., Delmotte, L., Martin, P., Ledred, R., Baron, J., Saehr, D., 1992. F-19
381 MAS-NMR STUDY OF STRUCTURAL FLUORINE IN SOME NATURAL AND
382 SYNTHETIC 2/1 LAYER SILICATES. Clay Clay Min. 40, 186-191.
383 Kalo, H., Milius, W., Brau, M., Breu, J., 2013. Synthesis and single crystal
384 structure refinement of the one-layer hydrate of sodium brittle mica. J. Solid State
385 Chem. 198, 57-64.
386 Kalo, H., Moller, M.W., Ziadeh, M., Dolejs, D., Breu, J., 2010. Large scale melt
387 synthesis in an open crucible of Na-fluorohectorite with superb charge homogeneity and
388 particle size. Appl. Clay Sci. 48, 39-45.
389 Kaviratna, H., Pinnavaia, T.J., 1994. ACID-HYDROLYSIS OF OCTAHEDRAL
390 MG2+ SITES IN 2/1 LAYERED SILICATES - AN ASSESSMENT OF EDGE
391 ATTACK AND GALLERY ACCESS MECHANISMS. Clay Clay Min. 42, 717-723.
392 Keenan, C.D., Herling, M.M., Siegel, R., Petzold, N., Bowers, C.R., Rössler, E.A.,
393 Breu, J., Senker, J., 2013. Porosity of Pillared Clays Studied by Hyperpolarized Xe-129
394 NMR Spectroscopy and Xe Adsorption Isotherms. Langmuir 29, 643-652.
395 Kitajima, K., Daimon, N., 1972. STUDIES ON SWELLING OF NA-
396 TAENIOLITE WITH WATER. Chem. Lett., 953-956.
397 Kitajima, K., Koyama, F., Takusagawa, N., 1985. SYNTHESIS AND SWELLING
398 PROPERTIES OF FLUORINE MICAS WITH VARIABLE LAYER CHARGES. Bull.
399 Chem. Soc. Jpn. 58, 1325-1326.

Kitajima, K., Sugimori, K., Daimon, N., 1973. STUDIES OF SWELLING OF NA-TAENIOLITE WITH WATER. Nippon Kagaku Kaishi, 1885-1892.

Kitajima, K., Takusagawa, N., 1990. EFFECTS OF TETRAHEDRAL ISOMORPHIC SUBSTITUTION ON THE IR-SPECTRA OF SYNTHETIC FLUORINE MICAS. Clay Min. 25, 235-241.

Kitajima, K., Taruta, S., Takusagawa, N., 1991. EFFECTS OF LAYER CHARGE ON THE IR-SPECTRA OF SYNTHETIC FLUORINE MICAS. Clay Min. 26, 435-440.

Komarneni, S., Ravella, R., Park, M., 2005. Swelling mica-type clays: synthesis by NaCl melt method, NMR characterization and cation exchange selectivity. J. Mater. Chem. 15, 4241-4245.

Kondo, R., Daimon, M., Asaga, K., Nishikawa, T., Kitajima, K., Daimon, N., 1980. SOLID-SOLUTIONS IN THE SYSTEM TAENIOLITE-SODIUM TAENIOLITE AND THEIR PROPERTIES. J. Am. Ceram. Soc. 63, 41-43.

Kunz, D.A., Schmid, J., Feicht, P., Erath, J., Fery, A., Breu, J., 2013. Clay-Based Nanocomposite Coating for Flexible Optoelectronics Applying Commercial Polymers. ACS Nano 7, 4275-4280.

Labouriau, A., Kim, Y.W., Chipera, S., Bish, D.L., Earl, W.L., 1995. A F-19 nuclear magnetic resonance study of natural clays. Clay Clay Min. 43, 697-704.

Lagaly, C., 1994. Layer Charge Determination by Alkylammonium Ions., in: Society, C.M. (Ed.), Layer Charge Characteristics of 2:1 Silicates Clay Minerals. CMS Workshop Lecture, Boulder Colorado, pp. 2-46.

Lezhnina, M., Benavente, E., Bentlage, M., Echevarría, Y., Klumpp, E., Kynast, U., 2007. Luminescent Hybrid Material Based on a Clay Mineral. Chem. Mat. 19, 1098-1102.

425 Mallouk, T.E., Gavin, J.A., 1998. Molecular recognition in lamellar solids and thin
426 films. Accounts Chem. Res. 31, 209-217.
427 Mariychuk, R., Baumgartner, A., Wagner, F.E., Lerf, A., Dubbe, A., Moos, R.,
428 Breu, J., 2007. Synthesis, structure, and electric conductivity of ferrous tainiolite and its
429 oxidative conversion into coarse-grained swellable smectite. Chem. Mat. 19, 5377-
430 5387.
431 Massiot, D., Fayon, F., Capron, M., King, I., Le Calve, S., Alonso, B., Durand,
432 J.O., Bujoli, B., Gan, Z.H., Hoatson, G., 2002. Modelling one- and two-dimensional
433 solid-state NMR spectra. Magn. Reson. Chem. 40, 70-76.
434 Mercier, L., Pinnavaia, T.J., 1998. A functionalized porous clay heterostructure for
435 heavy metal ion (Hg2+) trapping. Microporous Mesoporous Mat. 20, 101-106.
436 Miyake, M., Suzuki, T., Suzuki, T., 1993. CATION-EXCHANGE SELECTIVITY
437 FOR K+, MG2+, AND CA2+ IONS ON SODIUM-SUBSTITUTED TAENIOLITE.
438 Chem. Mat. 5, 1327-1331.
439 Moller, M.W., Hirsemann, D., Haarmann, F., Senker, J., Breu, J., 2010. Facile
440 Scalable Synthesis of Rectorites. Chem. Mat. 22, 186-196.
441 Moore, G.J., Zavalij, P.Y., Whittingham, M.S., 1997. Fluorophlogopite and
442 taeniolite: Synthesis and nanocomposite formation, in: Komarneni, S., Parker, J.C.,
443 Wollenberger, H.J. (Eds.), Nanophase and Nanocomposite Materials Ii. Materials
444 Research Society, Warrendale, pp. 501-506.
445 Muller, F., Besson, G., Manceau, A., Drits, V.A., 1997. Distribution of
446 isomorphous cations within octahedral sheets in montmorillonite from Camp-Bertaux.
447 Phys. Chem. Miner. 24, 159-166.

448 Naranjo, M., Castro, M.A., Cota, A., Osuna, F.J., Pavon, E., Alba, M.D., 2015.
449 Synthesis temperature effect on Na-Mica-4 crystallinity and heteroatom distribution.
450 Microporous Mesoporous Mat. 204, 282-288.
451 Okada, T., Ogawa, M., 2017. Adsorbents Derived from Layered Solids, in: Nakato,
452 T., Kawamata, J., Takagi, S. (Eds.), Inorganic Nanosheets and Nanosheet-Based
453 Materials: Fundamentals and Applications of Two-Dimensional Systems. Springer
454 Japan, Tokyo, pp. 263-301.
455 Park, M., Lee, D.H., Choi, C.L., Kim, S.S., Kim, K.S., Choi, J., 2002. Pure Na-4-
456 mica: Synthesis and characterization. Chem. Mat. 14, 2582-2589.
457 Paulus, W.J., Komarneni, S., Roy, R., 1992. BULK SYNTHESIS AND
458 SELECTIVE EXCHANGE OF STRONTIUM IONS IN NA4MG6AL4SI4O20F4
459 MICA. Nature 357, 571-573.
460 Pavon, E., Castro, M.A., Cota, A., Osuna, F.J., Pazos, M.C., Alba, M.D., 2014.
461 Interaction of Hydrated Cations with Mica-n (n=2, 3 and 4) Surface. J. Phys. Chem. C
462 118, 2115-2121.
463 Pavon, E., Castro, M.A., Naranjo, M., Orta, M.M., Pazos, M.C., Alba, M.D., 2013.
464 Hydration properties of synthetic high-charge micas saturated with different cations: An
465 experimental approach. Am. Miner. 98, 394-400.
466 Rayner-Canham, A.G., Overton, T., 2006. Descriptive Inorganic Chemistry, 4th ed.
467 Freeman, New York.
468 Sanz, J., Robert, J.L., Diaz, M., Sobrados, I., 2006. Influence of charge location on
469 Si-29 NMR chemical shift of 2 : 1 phyllosilicates. Am. Miner. 91, 544-550.
470 Schollhorn, R., 1996. Intercalation systems as nanostructured functional materials.
471 Chem. Mat. 8, 1747-1757.

Schoonheydt, R.A., Umemura, Y., 2017. Clay Minerals as Natural Nanosheets, in: Nakato, T., Kawamata, J., Takagi, S. (Eds.), Inorganic Nanosheets and Nanosheet-Based Materials: Fundamentals and Applications of Two-Dimensional Systems. Springer Japan, Tokyo, pp. 33-53.

Sposito, G., Prost, R., 1982. STRUCTURE OF WATER ADSORBED ON SMECTITES. Chem. Rev. 82, 553-573.

Suzuki, N., Komuro, T., Kanzaki, Y., 2008. Interfering effect for the cesium ion-exchange property of sodium difluorotetrasilicate and sodium taeniolite by alkaline-earth metal ions. Bull. Chem. Soc. Jpn. 81, 912-916.

Thomas, J.M., 1988. UNIFORM HETEROGENEOUS CATALYSTS - THE ROLE OF SOLID-STATE CHEMISTRY IN THEIR DEVELOPMENT AND DESIGN. Angew. Chem.-Int. Edit. 27, 1673-1691.

Tomohiko, O., Yoko, S., Makoto, O., 2014. Designed nanostructures of clay for controlled adsorption of organic compounds. Journal of Nanoscience and Nanotechnology 14, 2121-2134.

Toraya, H., Iwai, S., Marumo, F., Hirao, M., 1977. CRYSTAL-STRUCTURE OF TAENIOLITE, KLIMG2SI4O10F2. Z. Kristall. 146, 73-83.

Vaccari, A., 1999. Clays and catalysis: a promising future. Appl. Clay Sci. 14, 161-198.

Welch, M.D., Liu, S.X., Klinowski, J., 1998. Si-29 MAS NMR systematics of calcic and sodic-calcic amphiboles. Am. Miner. 83, 85-96.

Yamaguchi, T., Ikuta, K., Taruta, S., Kitajima, K., 2012. Morphology control and interlayer pillaring of swellable Na-taeniolite mica crystals. Mater. Sci. Eng. B-Adv. Funct. Solid-State Mater. 177, 524-527.